

# On Stability Analysis of Power Grids with Synchronous Generators and Grid-Forming Converters under DC-side Current Limitation

Sayan Samanta<sup>1</sup> and Nilanjan Ray Chaudhuri<sup>1</sup>

**Abstract**—Stability of power grids with synchronous generators (SGs) and renewable generation interfaced with grid-forming converters (GFCs) under dc-side current limitation is studied. To that end, we first consider a simple 2-bus test system and reduced-order models to highlight the fundamental difference between two classes of GFC controls – (A) droop, dispatchable virtual oscillator control (dVOC) and virtual synchronous machine (VSM), and (B) matching control. Next, we study Lyapunov stability and input-output stability of the dc voltage dynamics of class-A GFCs for the simple system and extend it to a generic system. Next, we provide a sufficiency condition for input-to-state stability of the 2-bus system with a class-B GFC and extend it for a generic system. Finally, time-domain simulations from a reduced-order averaged model of the simple test system and a detailed switched model of the GFC validate the proposed conditions.

## I. INTRODUCTION

Although a lot of intellectual capital has been invested towards research on prospective grids with 100% converter-based generation – it is of the authors' opinion that such systems may not become a reality as far as bulk power systems are concerned. Bulk power grids of the near and even distant future are expected to have SGs in them, since hydro, solar thermal, and nuclear power are all here to stay. Indeed, many studies have been performed on the penetration of converter-based resources in presence of SGs, e.g. [1], [2] and references therein, which in spite of their obvious merit, lack analytical insights that are fundamental to identifying major challenges in modeling and control of such systems and develop new theories in solving them.

It is only in the recent past that these gaps and challenges were summarized in a comprehensive manner by Milano et al [3]. Among the multitude of fertile areas of research that can be pursued to solve these challenges, we focus on the dynamics, stability, and control of the real power channel in such systems that primarily affects the dc-link voltages of converter-based renewable generation and frequency of the ac system. To that end, we consider the GFC technology and its interaction with SGs in a bulk power grid, where two classes of GFC controls – (1) droop, dVOC and VSM [4]–[6] – we call it class-A, and (2) matching control [7] – we term it class-B, are compared.

Our research is motivated by two relatively new papers on this topic [8], [9]. In [8], modeling adequacy of such systems is established through singular perturbation theory –

our paper follows similar modeling guidelines. However, the control law assumed for governor action in SGs in [8] is not quite realistic. A more realistic turbine-governor dynamics is considered in a follow up paper [9]. This paper showed some interesting findings on frequency of ac system and dc voltage dynamics of GFCs in presence of dc-side and ac current limitations. It was demonstrated that in presence of dc-side current limit, the dc voltages of class-A GFCs can become unstable under large increase in load, while class-B GFCs demonstrate increased robustness in stability, since regulation of their ac side angle dynamics takes into account the dc voltage dynamics. However, analytical treatment of stability guarantees in presence of dc-side current limitations was reserved for future research. In addition, we feel that there is a need to complement the efforts in contrasting the basics of class-A and class-B GFCs in these papers by presenting the characteristics of class-A GFCs in the converter power–dc voltage plane and also bringing more clarity on their fundamental difference with the class-B counterpart.

Thus motivated, the objectives of this paper are twofold – (1) develop an understanding of the fundamental difference between the two classes of GFC controls; and (2) provide analytical guarantees of stability (for class-A and -B) and sufficiency conditions of instability (for class-A) in presence of dc-side current limitation, when such converters are connected to a power system with SG-based conventional generation. Presence of both ac and dc-side current limitations is considered out of scope for this work and will be reported in a future paper. Nevertheless, we have presented a discussion on this topic in Section III.C.

## II. CLASSES OF GFC CONTROLS: REDUCED-ORDER MODEL

A typical circuit diagram of a GFC interfacing renewable resources is shown in Fig. 1 whose dc bus is connected for example, to a PV solar unit or the dc side of ac-dc converter of a Type-4 wind turbine. Therefore, we restrict our focus to the dc to ac unidirectional power flow scenario, i.e. energy storage is excluded from our analysis. The notations associated with parameters and variables mentioned in this figure are standard and self-explanatory, see [10] for example.

The GFC is controlled in a synchronously rotating  $d-q$  reference frame whose angular frequency  $\omega_c$  is imposed by the converter. The standard inner current control, albeit without any limits and voltage control loops, common across class-A and class-B, are shown in Fig. 2. It is the outer loops where the GFC control strategies differ – for further details

<sup>1</sup>Sayan Samanta and Nilanjan Ray Chaudhuri are with The School of Electrical Engineering & Computer Science, The Pennsylvania State University, University Park, PA 16802, USA. [sps6260@psu.edu](mailto:sps6260@psu.edu), [nuc88@psu.edu](mailto:nuc88@psu.edu)

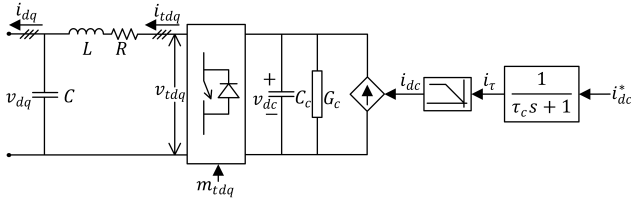


Fig. 1: Circuit diagram of GFC.

on class-A and class-B outer loops, the readers are referred to [8], [9].

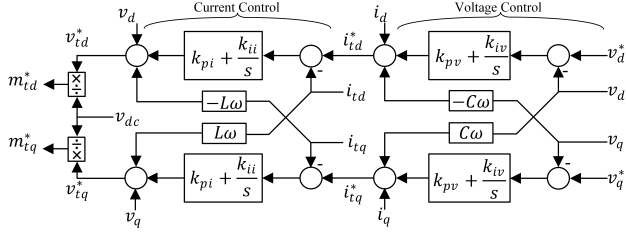


Fig. 2: Block diagram of voltage and current control loops.

First, we consider a simple test system shown in Fig. 3 with one SG and one GFC. Based upon modeling adequacy study presented in [8], we assume that the control loops shown in Fig. 2 track the references instantaneously, and the transmission dynamics and losses can be neglected. Moreover, since our focus is on the dynamics of the real power channel, we represent the dc-link dynamics of the GFC and the swing dynamics of the SG along with corresponding turbine-governor dynamics. Also, SGs are assumed to have adequate headroom to deliver any load change and a dc power flow assumption is made. Next, we present the reduced-order model of this system based on the time-scale separation of ac and dc dynamics [8], [9].

#### A. Reduced-order Model of Class-A GFCs

Neglecting the time constant  $\tau_c$  of the dc energy source in Fig. 1, we can derive the test system model with class-A GFC shown in Fig. 5(a):

$$\dot{v}_{dc} = \frac{1}{C_c} \left[ -G_c v_{dc} + \text{sat} \left( k_c (v_{dc}^* - v_{dc}), i_{dc}^{\max} \right) - \frac{P_c}{v_{dc}} \right] \quad (1a)$$

$$\dot{\phi} = \underline{\omega}_c - \underline{\omega}_g; \quad \underline{\omega}_c = -d_{pc} (P_c - P_c^*); \quad \underline{\omega}_g = \omega_g - \omega_g^* \quad (1b)$$

$$\underline{\omega}_g = \frac{1}{2H_g} [P_{\tau g} - P_g] \approx \frac{1}{2H_g} [P_{\tau g} + b\phi - P_{Lg}] \quad (1c)$$

$$\dot{P}_{\tau g} = \frac{1}{\tau_g} [P_g^* - d_{pg} \underline{\omega}_g - P_{\tau g}] \quad (1d)$$

where,  $c, g, \tau_g$ : subscripts corresponding to GFC, SG, and turbine-governor, \*: superscript for reference quantities,  $v_{dc}$ : dc-link voltage,  $C_c$ : dc-link capacitance,  $G_c$ : conductance representing dc-side losses,  $k_c$ : dc voltage droop constant,  $i_{dc}^{\max}$ : dc-side current limit reflecting the capacity of the renewable resource,  $P, P_L$ : real power output, load,  $\phi$ : angle difference between bus voltages of GFC and SG, i.e.,  $\phi = \theta_c - \theta_g$ ,  $d_{pc}$ : coefficient of droop/dVOC/VSM control,  $\omega$ : angular frequency,  $H_g$ : SG inertia constant,  $\tau_g$ : turbine time

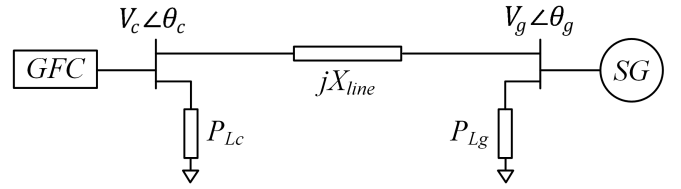


Fig. 3: Single-line diagram of the test system.

constant,  $d_{pg}$ : SG inverse governor droop, and  $b$ : transmission line susceptance.

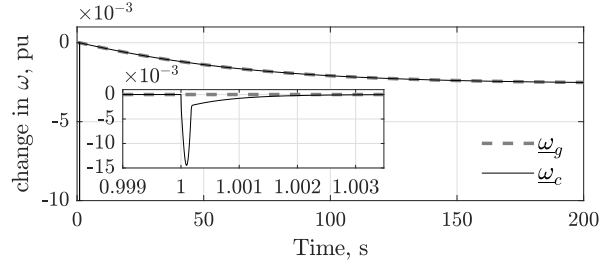


Fig. 4:  $\omega_g$  and  $\omega_c$  for class-B GFC

#### B. Reduced-order Model of Class-B GFCs

Modifying (1a) by including the feedforward terms considered in matching control as in [9], we can write:

$$C_c \dot{v}_{dc} = -G_c v_{dc} + \text{sat} \left( G_c v_{dc} + \frac{P_c^*}{v_{dc}^*} + k_c (v_{dc}^* - v_{dc}), i_{dc}^{\max} \right) - \frac{P_c}{v_{dc}} \quad (2)$$

With matching control law  $k_m v_{dc} = \omega_c$  and  $k_m v_{dc}^* = \omega^* = 1$  pu, we can modify (2) and (1)(b)-(d) to derive the test system model with class-B GFC, which is shown in Fig. 5(b). In presence of matching control, as the angle dynamics is very fast compared to the machine dynamics, a reasonable assumption is  $\omega_c \approx \omega_g \Rightarrow \underline{\omega}_c \approx \underline{\omega}_g = \omega_g - \omega^*$  [9]. This can be shown through time-domain simulation of Fig. 5(b) following a step change in  $P_{Lc}$ , which is highlighted in Fig. 4. Since  $\underline{\omega}_c$  and  $\underline{\omega}_g$  are indistinguishable with step change in  $P_{Lg}$ , it is not shown. With this approximation, we can write:

$$\begin{aligned} \frac{C_c}{k_m^2} \dot{\underline{\omega}}_g &= \text{sat} \left( -\frac{k_c}{k_m^2} \underline{\omega}_g, \underline{P}_c^{\max} \right) + P_c^* - P_c \frac{\omega^*}{\omega_g} \\ &\approx \text{sat} \left( -d_{pc} \underline{\omega}_g, \underline{P}_c^{\max} \right) - \underline{P}_c \end{aligned} \quad (3)$$

With  $\frac{C_c}{k_m^2} \approx 0$  as assumed in [9], we can write:

$$\underline{P}_c = -\text{sat} \left( d_{pc} \underline{\omega}_g, \underline{P}_c^{\max} \right) \quad (4)$$

where,  $d_{pc} = \frac{k_c}{k_m^2}$ ,  $\underline{P}_c^{\max} = v_{dc}^* i_{dc}^{\max} - G_c v_{dc}^{*2} - P_c^*$ ,  $\underline{P}_c = P_c - P_c^*$ . With total load in the system  $P_L = P_{Lg} + P_{Lc}$  and power balance under nominal condition, i.e.  $-P_g^* - P_c^* + P_L^* = 0$ , we can write:

$$\begin{aligned} \dot{\underline{\omega}}_g &= \frac{1}{2H_g} (\underline{P}_{\tau g} - \text{sat} (d_{pc} \underline{\omega}_g, \underline{P}_c^{\max}) - \underline{P}_L) \\ \dot{\underline{P}}_{\tau g} &= \frac{1}{\tau_g} (-\underline{P}_{\tau g} - d_{pg} \underline{\omega}_g) \end{aligned} \quad (5)$$

where,  $\underline{P}_{\tau g} = P_{\tau g} - P_g^*$  and  $\underline{P}_L = P_L - P_L^*$ .

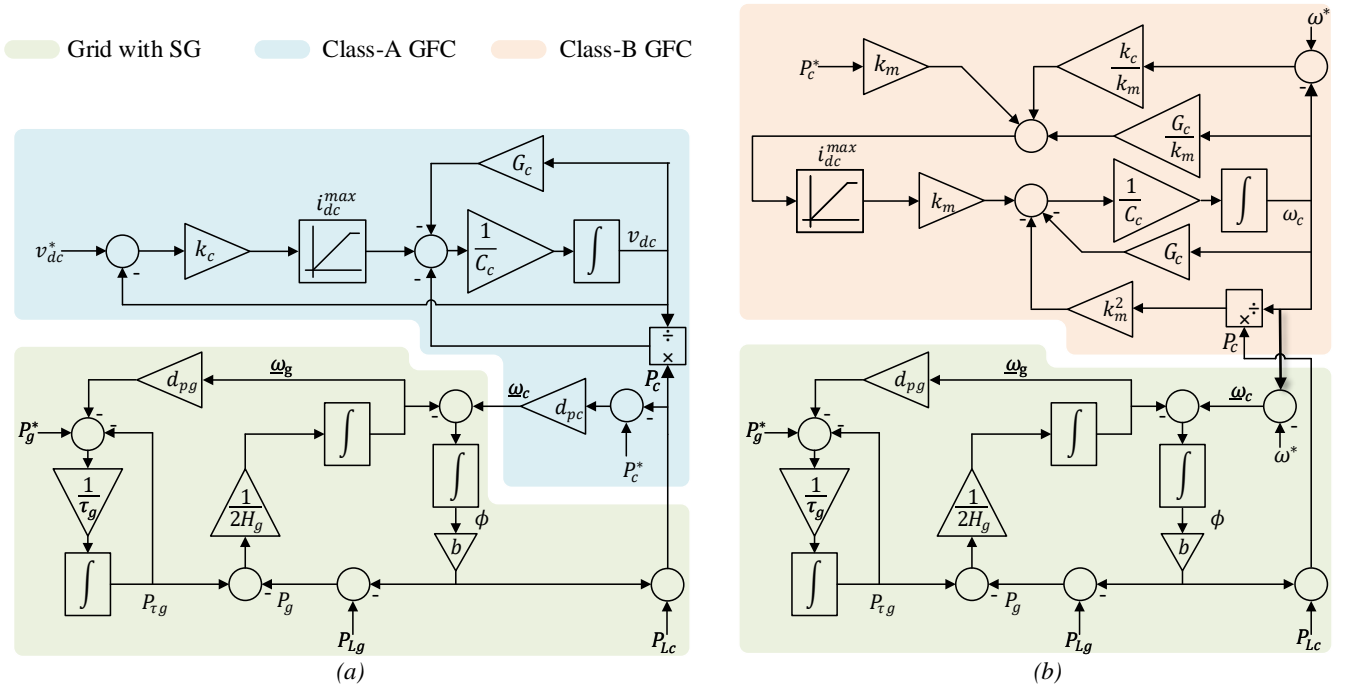


Fig. 5: Block diagram of simplified mathematical models of the test system in Fig. 3 for: (a) Class-A GFCs (droop, dVOC, VSM control) and (b) Class-B GFCs (matching control): feedback path from GFC to grid is highlighted.

### C. Discussion on Fundamental Difference between Class-A and Class-B GFCs

The model of class-A GFCs in (1) is shown in a block diagram form in Fig. 5(a). The most striking aspect of this class of control is that it merely acts as a buffer to adjust the frequency of its terminal voltage in order to deliver the power  $P_c$  demanded by the system, which in turn affects the dc-link voltage dynamics. The converter has no direct control over  $P_c$  and the dc-link dynamics does not have any ‘feedback mechanism’ to alter it. Therefore, the stability of the dc-link voltage of class-A GFCs described by (1a) can be analyzed in isolation. Let,  $v_{dc} = x > 0$ ,  $v_{dc}^* = x^*$ ,  $P_c = u > 0$ , and  $(\bar{x}, \bar{u})$ ,  $\bar{x} > 0, \bar{u} > 0$  be the equilibrium point. Also, assume  $x^*$  is chosen such that the allowable maximum value of  $x$  is  $\tilde{x}^* = \frac{k_c}{(k_c + G_c)} x^*$ , i.e. when  $x \rightarrow \tilde{x}^*$ , protective circuits will kick in and limit the dc voltage. Define,  $y = x - \bar{x} \Rightarrow x = y + \bar{x}$ ,  $v = u - \bar{u} \Rightarrow u = v + \bar{u}$ . Now, (1a) can be written as:

$$\dot{y} = \frac{1}{C_c} [-G_c(y + \bar{x}) + \text{sat}(k_c(x^* - y - \bar{x}), i_{dc}^{max}) - \frac{v + \bar{u}}{y + \bar{x}}] \quad (6)$$

This equation is in the form  $\dot{y} = f(y, v)$ ,  $y = h(y)$ , where  $f: D_y \times D_v \rightarrow \mathbb{R}$  is locally Lipschitz in  $(y, v)$ ,  $h: D_y \rightarrow D_y$  is continuous in  $(y, v)$ ,  $f(0, 0) = 0$ , and domains  $D_y = (-\bar{x}, \tilde{x}^* - \bar{x}) \subset \mathbb{R}$ ,  $D_v \subset \mathbb{R}$  contain the origin. The equilibrium  $(\bar{x}, \bar{u})$  satisfies the following equation:

$$\bar{u} = \begin{cases} f_1: -G_c \bar{x}^2 + k_c \bar{x}(x^* - \bar{x}), & \text{if } |k_c(x^* - \bar{x})| \leq i_{dc}^{max} \\ f_2: -G_c \bar{x}^2 + \bar{x} i_{dc}^{max}, & \text{otherwise} \end{cases}$$

Depending upon the value of  $x$  where the maxima of  $\bar{u}$  is found, we can get four types of characteristics in  $x - u$  plane

as shown in Fig. 6. Out of these, the typical case is that in Fig. 6(a) – going forward, unless otherwise mentioned, we will consider this characteristic. We note that for any given  $\bar{u}$ , there exists two equilibria  $\bar{x}_1 \in \Omega_1 = [x_m, \tilde{x}^*]$  and  $\bar{x}_2 \in \Omega_2 = (0, x_m]$ , where  $x_m = x^* - \frac{i_{dc}^{max}}{k_c}$ .

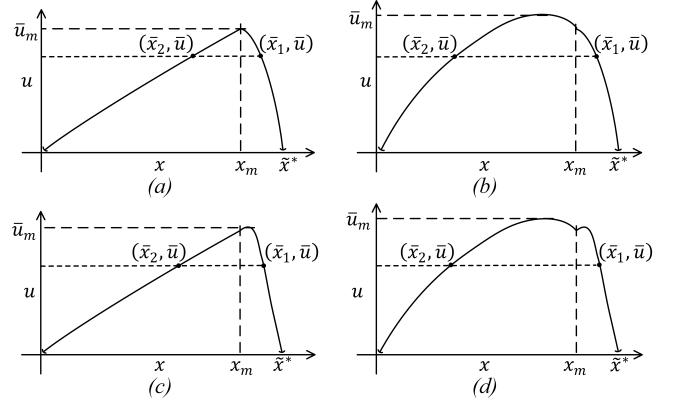


Fig. 6: Four possible  $u$  vs  $x$  characteristics.

In contrast, the model of class-B GFCs before reduction to the form in (5) is shown in Fig. 5(b). The most important difference with respect to its class-A counterpart is that it has a ‘feedback mechanism’ from the dc-link voltage dynamics to the rest of the system that can alter the power  $P_c$  demanded from the GFC. Thus, the stability of dc-link voltage can not be analyzed in isolation and a reduced-order model in (5) is used for this purpose. Assuming  $z = [\omega_g \ P_{\tau g}]^T$ ,  $w = -P_L$ , (5) can be expressed as  $\dot{z} = g(z, w)$ ,  $g: \mathbb{R}^2 \times \mathbb{R} \rightarrow \mathbb{R}^2$ , where  $g$

is locally Lipschitz in  $(z, w)$ , and  $g(0, 0) = 0$ . From a control design point of view, the fundamental difference between class-A and B can also be perceived as their dependency on either the ac or dc quantities [11], [12].

### III. STABILITY ANALYSIS IN PRESENCE OF DC-SIDE CURRENT LIMITS

We focus on stability analysis of  $v_{dc}$  in presence of dc-side current limits. To that end, we establish the following: (1) Lyapunov stability and region of attraction (ROA) for class-A and class-B GFCs, (2) Sufficiency condition for input-output stability for class-A GFCs, (3) Sufficiency condition for instability of class-A GFCs, and (4) Sufficiency condition for input-to-state stability for class-B GFCs.

#### A. Stability Analysis of Class-A GFC

We first focus on the reduced model of the 2-bus test system in Fig. 3 and present the following Theorems and Lemmas.

**Theorem III.1.** *For class-A GFCs, the equilibrium  $\bar{x}_1$  is asymptotically stable with ROA  $\mathcal{R}_A = (\bar{x}_2, \bar{x}^*)$ .*

*Proof.* Corresponding to the domain  $\Omega_1$  for  $x$ , (6) can be rewritten as:

$$\dot{y} = \frac{1}{C_c} \left[ -G_c y - k_c y + \frac{\bar{u}}{\bar{x}_1} \frac{y}{y + \bar{x}_1} - \frac{v}{y + \bar{x}_1} \right] \quad (7)$$

where,  $y \in \bar{D}_y = [x_m - \bar{x}_1, \bar{x}^* - \bar{x}_1] \subset D_y$ ,  $v \in D_v$ . Choosing a Lyapunov function  $V_1 = \frac{C_c}{2} y^2$ ,  $y \in \bar{D}_y$ , we can write for the unforced system:  $\dot{V}_1 = \left[ -(G_c + k_c) + \frac{\bar{u}}{\bar{x}_1} \frac{1}{y + \bar{x}_1} \right] y^2$ . It can be shown that  $\dot{V}_1$  is negative definite, if  $y > \bar{x}^* - 2\bar{x}_1$ . In the most typical case as in Fig. 6(a),  $\bar{x}_1 > x_m > \frac{\bar{x}^*}{2}$ , which satisfies this condition. Therefore,  $\bar{x}_1$  is asymptotically stable  $\forall x \in \Omega_1$ .

To establish the ROA of  $\bar{x}_1$ , we analyze Lyapunov stability of  $\bar{x}_2 \in \Omega_2$  shown in Fig. 6(a) with the same  $\bar{u}$ . To that end, we can rewrite (6) with  $v = 0$  as:  $\dot{y} = \frac{1}{C_c} \left[ -G_c(y + \bar{x}_2) + i_{dc}^{\max} - \frac{\bar{u}}{y + \bar{x}_2} \right]$ ,  $y \in \bar{D}_y = (-\bar{x}_2, x_m - \bar{x}_2]$ . Choosing a continuously differentiable function  $V_2 = \frac{C_c}{2} [\bar{x}_2^2 - (y + \bar{x}_2)^2]$ ,  $y \in \bar{D}_y$ , s.t.  $V_2(0) = 0$ . We choose a ball  $B_r = \{y \in \mathbb{R} \mid |y| \leq r\}$  and define set  $U = \{y \in B_r \mid V_2 > 0\}$  – note that  $U \subseteq (-\bar{x}_2, 0)$ . Therefore, we can choose  $y(0) = y_0 \in U$  arbitrarily close to the origin s.t.  $V_2(y_0) > 0$ . Also,  $\dot{V}_2 > 0, \forall y \in U$ , if  $y < \frac{i_{dc}^{\max}}{G_c} - 2\bar{x}_2$ . Taking into account the typical characteristics in Fig. 6(a) and analyzing local maxima of  $f_2$ , we can write  $\frac{i_{dc}^{\max}}{2G_c} > \bar{x}_2$ . Therefore,  $\dot{V}_2 > 0, \forall y \in U$ , which provides a sufficiency condition for instability of  $\bar{x}_2$  following Chetaev's theorem [13]. This implies that  $x(t)$  with any initial value  $x(0) = x_0 \in (0, \bar{x}_2) \subset \Omega_2$  will move away from  $\bar{x}_2$  and reach 0.

Next, choosing a continuously differentiable function  $V_3 = \frac{C_c}{2} [(y + \bar{x}_2)^2 - \bar{x}_2^2]$ ,  $y \in \bar{D}_y$ , s.t.  $V_3(0) = 0$  – it is easy to follow similar arguments and show that  $V_3 > 0, \forall y \in (0, x_m - \bar{x}_2] \subset \bar{D}_y$ . This implies that  $x(t)$  with any initial value  $x_0 \in \bar{\Omega}_2 = (\bar{x}_2, x_m] \subset \Omega_2$  will move away from  $\bar{x}_2$  and reach  $x_m$ .

We define  $\mathcal{R}_A = \bar{\Omega}_2 \cup \Omega_1 = (\bar{x}_2, \bar{x}^*)$ , which is the largest open, connected, invariant set in  $\Omega_2 \cup \Omega_1$ , such that  $\lim_{t \rightarrow \infty} x(t) = \bar{x}_1, \forall x(0) \in \mathcal{R}_A$ . This implies  $\mathcal{R}_A$  is the ROA for equilibrium  $\bar{x}_1$  of class-A GFCs.  $\square$

**Corollary III.1.1.** *For class-A GFCs, the equilibrium  $\bar{x}_1$  is exponentially stable in  $\Omega_1$ .*

*Proof.* As mentioned in Theorem III.1, the chosen Lyapunov function is  $V_1 = \frac{C_c}{2} y^2 = \frac{C_c}{2} |y|^2, y \in \bar{D}_y$ . Also,  $\dot{V}_1 \leq \left[ -(G_c + k_c) + \frac{\bar{u}}{\bar{x}_1} \frac{1}{x_m} \right] |y|^2, y \in \bar{D}_y$ . Since,  $m = -(G_c + k_c) + \frac{\bar{u}}{\bar{x}_1} \frac{1}{x_m} < 0$ , it satisfies all conditions in Theorem 4.10 in [13], and therefore  $\bar{x}_1$  is exponentially stable in  $\Omega_1$ .  $\square$

**Theorem III.2.** *The dc voltage dynamics of class-A GFCs described in (6) is small-signal finite-gain  $\mathcal{L}_p$  stable  $\forall p \in [1, \infty]$ , if  $y(0) = y_0 \in \{|y| \leq r\} \subset \bar{D}_y$ ,  $r > 0$ . Also, for a  $r_v > 0$ , s.t.  $\{|v| \leq r_v\} \subset D_v$ ,  $r_v > 0, \forall v \in \mathcal{L}_{pe}$  with  $\sup_{0 \leq t \leq \tau} |v| \leq \min\{r_v, |m|x_m r\}$ , the output  $y(t)$  is bounded by the following relation  $\|y\tau\|_{\mathcal{L}_p} \leq \frac{\|v\tau\|_{\mathcal{L}_p}}{|m|x_m} + \beta \quad \forall \tau \in [0, \infty)$ , where  $\beta = |y_0|$ , if  $p = \infty$ , and  $\left(\frac{C_c}{p|m}\right)^{\frac{1}{p}} |y_0|$ , if  $p \in [1, \infty)$ .*

*Proof.* We proved that  $y = 0$  is exponentially stable in  $\bar{D}_y$  in Corollary III.1.1. With Lyapunov function  $V_1 = \frac{C_c}{2} y^2 = \frac{C_c}{2} |y|^2$ , we have  $\dot{V}_1 \leq -|m||y|^2$ ,  $\left| \frac{\partial V_1}{\partial y} \right| = C_c |y|$ ,  $\forall y \in \bar{D}_y$ . Also,  $|f(y, v) - f(y, 0)| \leq \frac{1}{C_c x_m} |v|$ ,  $|h(y, v)| = |y|$ ,  $\forall y \in \bar{D}_y, \forall v \in D_v$ . This satisfies all conditions in Theorem 5.1 in [13] and proves the conditions for input-output stability and bound on output.  $\square$

**Theorem III.3.** *For class-A GFCs, the equilibrium  $\bar{x}_1 \in \Omega_1$  of (6) with  $v = 0$  is unstable if  $\bar{u} > -G_c(y + \bar{x}_1)^2 + (y + \bar{x}_1) \text{sat}(k_c(x^* - y - \bar{x}_1), i_{dc}^{\max})$  for any  $y \in [-r, 0)$ , where  $r = \min\{\bar{x}_1, \bar{x}^* - \bar{x}_1\}$ .*

*Proof.* The unforced system can be expressed as  $\dot{y} = \frac{1}{C_c} [-G_c(y + \bar{x}_1) + \text{sat}(k_c(x^* - y - \bar{x}_1), i_{dc}^{\max}) - \frac{\bar{u}}{y + \bar{x}_1}]$ ,  $\forall y \in D_y \subset \mathbb{R}$ . Define a continuously differentiable function,  $V_4 : D_y \rightarrow \mathbb{R}$ ,  $V_4(y) = \frac{1}{2} C_c [\bar{x}_1^2 - (y + \bar{x}_1)^2]$  such that  $V_4(0) = 0$ . Choose  $r \in (0, \min\{\bar{x}_1, \bar{x}^* - \bar{x}_1\})$  such that the ball  $B_r = \{y \in \mathbb{R} \mid |y| \leq r\}$ ,  $B_r \subset D_y$ . Define,  $U = \{y \in B_r \mid V_4(y) > 0\}$ , implying  $U = [-r, 0)$ . Choose  $y_0$  in the interior of  $U \implies y_0 < 0$ . Hence,  $V_4(y_0) > 0$  for any such  $y_0$  arbitrarily close to the origin. Now, derivative of  $V_4$  along the trajectory of  $y$  is:

$$\dot{V}_4 = G_c(y + \bar{x}_1)^2 - (y + \bar{x}_1) \text{sat}(k_c(x^* - y - \bar{x}_1), i_{dc}^{\max}) + \bar{u}$$

According to Chetaev's theorem [13], the sufficiency condition for instability is  $\dot{V}_4 > 0, \forall y \in U$ , which proves the theorem.  $\square$

Now, we extend these proofs for a generic system with  $m_1$  SGs and  $n_1$  class-A GFCs, and introduce the following Corollary.

**Corollary III.3.1.** *Theorems III.1, III.2, III.3 and Corollary III.1.1 hold for any generic system.*

*Proof.* Discussions from Section II-C establish that the stability properties investigated in these theorems are independent of the systems as long as the GFC-level assumptions

taken in Section II hold. Therefore, these theorems and the corollary hold individually for each of the  $n_1$  class-A GFCs.  $\square$

### B. Stability Analysis of Class-B GFC

In this section, we first analyze the stability of class-B GFCs for the 2-bus system shown in Fig. 3 and present the following lemma and theorem.

**Lemma III.4.** *For class-B GFCs, the equilibrium  $z = 0$  is globally asymptotically stable  $\forall d_{pg}, d_{pc} > 0$ .*

*Proof.* For unforced system,  $w = -P_L = 0$ . Choose Lyapunov function with  $d_{pg} > 0$ ,  $V_5 = H_g \underline{\omega}_g + \frac{\tau_g}{2d_{pg}} P_{\tau_g}^2$ .

$$\Rightarrow \dot{V}_5 = -\frac{P_{\tau_g}^2}{d_{pg}} - \underline{\omega}_g \text{sat}(d_{pc} \underline{\omega}_g, \underline{P}_c^{\max})$$

Here,  $\underline{\omega}_g \text{sat}(d_{pc} \underline{\omega}_g, \underline{P}_c^{\max}) > 0 \quad \forall \underline{\omega}_g \in \mathbb{R} - \{0\}, d_{pc} > 0$ . Thus,  $\dot{V}_5$  is negative definite and radially unbounded  $\forall d_{pg}, d_{pc} > 0$ . Therefore, the origin is globally asymptotically stable when this condition is satisfied.  $\square$

*Remark.* We observe that the ROA for  $y = 0$  corresponding to the equilibrium  $\bar{x}_1$  of class-A GFCs is limited to  $y \in (\bar{x}_2 - \bar{x}_1, \bar{x}^* - \bar{x}_1)$ , while the same for  $z = 0$  of class-B GFCs is  $\mathbb{R}^2$ . Also, equilibrium  $\bar{x}_2$  of class-A GFCs is unstable.

**Theorem III.5.** *The reduced-order model (5) is input-to-state stable with class  $\mathcal{KL}$  function  $\beta$  and class  $\mathcal{K}$  function  $\gamma(|w|) = c \max\{\chi_1(|w|), \chi_2(|w|)\}$ ,  $c > 0$  for piecewise continuous  $w(t)$  that is bounded in  $t$ ,  $\forall t \geq 0$  implying  $\|z(t)\| \leq \beta(\|z(t_0)\|, t - t_0) + \gamma\left(\sup_{\tau \geq t_0} |w(\tau)|\right)$ ,  $\forall t \geq t_0$*

– where,  $\chi_1(|w|) = \frac{P_{\tau_g}^{\max}}{d_{pc}} \tanh^{-1}\left(\frac{|w|}{\theta \underline{P}_c^{\max}}\right)$  and  $\chi_2(|w|) = \left[\frac{|w| d_{pg}}{\theta} \chi_1(|w|)\right]^{\frac{1}{2}}$ ,  $\forall w \in (-\theta \underline{P}_c^{\max}, \theta \underline{P}_c^{\max})$ ,  $\underline{P}_c^{\max} \in \mathbb{R}_{>0}$ ,  $0 < \theta < 1$ ,  $\mathbb{R}_{>0}$ : positive real space.

*Proof.* In Lemma III.4, it is shown that  $\dot{z} = g(z, 0)$  is globally asymptotically stable. It can be shown that the Lyapunov function  $V_5(z)$  satisfies the following inequalities:  $\lambda_{\min}(Q) \|z\|_2^2 \leq V_5(z) \leq \lambda_{\max}(Q) \|z\|_2^2$ , which implies  $\alpha_1(\|z\|) \leq V_5(z) \leq \alpha_2(\|z\|)$ , where  $\alpha_1$  and  $\alpha_2$  are class  $\mathcal{K}_\infty$  functions and  $Q = \begin{bmatrix} H_g & 0 \\ 0 & \frac{\tau_g}{2d_{pg}} \end{bmatrix}$ . For  $0 < \theta < 1$ , we can write:

$$\begin{aligned} \dot{V}_5 &= -\frac{P_{\tau_g}^2}{d_{pg}} - \underline{\omega}_g \text{sat}(d_{pc} \underline{\omega}_g, \underline{P}_c^{\max}) + w \underline{\omega}_g \\ &\leq -(1 - \theta) \left( \frac{P_{\tau_g}^2}{d_{pg}} + \underline{\omega}_g \text{sat}(d_{pc} \underline{\omega}_g, \underline{P}_c^{\max}) \right) \\ &\quad - \theta \left( \frac{P_{\tau_g}^2}{d_{pg}} + \underline{\omega}_g \text{sat}(d_{pc} \underline{\omega}_g, \underline{P}_c^{\max}) \right) + |w| |\underline{\omega}_g| \end{aligned}$$

Let us define,  $W = (1 - \theta) \left( \frac{P_{\tau_g}^2}{d_{pg}} + \underline{\omega}_g \text{sat}(d_{pc} \underline{\omega}_g, \underline{P}_c^{\max}) \right)$ , which is a positive definite function in  $\mathbb{R}^2$ . Now, define  $\Gamma = -\theta \left( \frac{P_{\tau_g}^2}{d_{pg}} + \underline{\omega}_g \text{sat}(d_{pc} \underline{\omega}_g, \underline{P}_c^{\max}) \right) + |w| |\underline{\omega}_g|$ . The term  $\Gamma$

will be  $\leq 0$  if  $|\underline{\omega}_g| \geq \frac{\underline{P}_c^{\max}}{d_{pc}} \tanh^{-1}\left(\frac{|w|}{\theta \underline{P}_c^{\max}}\right) = \chi_1(|w|)$  or  $|\underline{\omega}_g| \leq \chi_1(|w|)$  and  $|\underline{P}_{\tau_g}| \geq \left[\frac{|w| d_{pg}}{\theta} \chi_1(|w|)\right]^{\frac{1}{2}} = \chi_2(|w|)$ . This condition implies  $\|z\|_\infty \geq \max\{\chi_1(|w|), \chi_2(|w|)\} = \rho(|w|)$ . So,

$$\dot{V}_5 \leq -W, \quad \forall \|z\|_\infty \geq \rho(|w|)$$

Here,  $\rho(|w|)$  is a class  $\mathcal{K}$  function with  $w \in (-\theta \underline{P}_c^{\max}, \theta \underline{P}_c^{\max})$ . Since,  $\underline{P}_c^{\max} \in \mathbb{R}_{>0}$ , we contend that the above holds  $\forall (z, w) \in \mathbb{R}^2 \times \mathbb{R}$ . Therefore, we have satisfied all conditions of input-to-state stability per Theorem 4.19 in [13].

Now, we need to define class  $\mathcal{K}$  function  $\gamma = \alpha_1^{-1} \circ \alpha_2 \circ \rho$ . It can be shown that  $\gamma(|w|) = \sqrt{\frac{\lambda_{\max}(Q)}{\lambda_{\min}(Q)}} \rho(|w|) = c \rho(|w|)$ .  $\square$

Next, we extend these proofs for a generic system with  $m_1$  SGs,  $n_1$  class-B GFCs, and  $p_1$  load buses. We assume that the center-of-inertia (COI) of this system is representative of its average frequency dynamics and the corresponding frequency  $\omega_{COI} \approx \omega_{ci}$ ,  $\forall i = 1, 2, \dots, n_1$ . Following the same approach as in Section II-B, we can present the reduced-order model of this system:

$$\begin{aligned} \dot{\omega}_{COI} &= \frac{1}{2H_T} \left[ P_{\tau_g T} - \sum_{i=1}^{n_1} \text{sat}(d_{pci} \omega_{COI}, \underline{P}_{ci}^{\max}) - P_{LT} \right] \\ \dot{P}_{\tau_g T} &= \frac{1}{\tau_{gT}} \left[ -P_{\tau_g T} - d_{pgT} \omega_{COI} \right] \end{aligned} \quad (8)$$

Here,  $H_T = \sum_{i=1}^{m_1} H_{gi}$ ,  $P_{\tau_g T} = \sum_{i=1}^{m_1} P_{\tau_g i}$ ,  $P_{gT}^* = \sum_{i=1}^{m_1} P_{gi}^*$ ,  $d_{pgT} = \sum_{i=1}^{m_1} d_{pgi}$ ,  $\tau_{gi} = \tau_{gT} \forall i$ ,  $P_{LT} = \sum_{i=1}^{p_1} P_{Li}$ ,  $\omega_{COI} = \omega_{COI} - \omega^*$ ,  $\underline{P}_{\tau_g T} = P_{\tau_g T} - P_{gT}^*$ ,  $\underline{P}_{LT} = P_{LT} - P_{LT}^*$ . Assuming  $z_1 = [\omega_{COI} \quad \underline{P}_{\tau_g T}]^T$ ,  $w_1 = -\underline{P}_{LT}$ , (8) can be expressed as  $\dot{z}_1 = g_1(z_1, w_1)$ ,  $g_1: \mathbb{R}^2 \times \mathbb{R} \rightarrow \mathbb{R}^2$ , where  $g_1$  is locally Lipschitz in  $(z_1, w_1)$ , and  $g_1(0, 0) = 0$ . We present the following lemma to analyze Lyapunov stability of this system.

**Lemma III.6.** *For class-B GFCs, the equilibrium  $z_1 = 0$  is globally asymptotically stable  $\forall d_{pgT}, d_{pci} > 0, \forall i$ .*

*Proof.* It is a simple extension of Lemma III.4. We use the Lyapunov function  $V_6 = H_T \omega_{COI}^2 + \frac{\tau_{gT}}{2d_{pgT}} P_{\tau_g T}^2$  with  $d_{pgT} > 0$  and notice that  $\sum_{i=1}^{n_1} \omega_{COI} \text{sat}(d_{pci} \omega_{COI}, \underline{P}_{ci}^{\max}) > 0 \quad \forall \omega_{COI} \in \mathbb{R} - \{0\}, d_{pci} > 0 \forall i$ , which proves the Lemma.  $\square$

Next, we present a corollary relating the input-to-state stability of this system.

**Corollary III.6.1.** *Theorem III.5 can be extended for establishing the input-to-state stability of (8) with the following modifications: (1)  $\underline{P}_{ci}^{\max}$  and  $d_{pc}$  correspond to the minimum value of  $\underline{P}_{ci}^{\max} \tanh\left(\frac{d_{pci}}{\underline{P}_{ci}^{\max}} \omega_{COI}\right)$ ,  $\forall i = 1 : n_1$ , (2)  $\chi_1(|w_1|) = \frac{\underline{P}_{ci}^{\max}}{d_{pc}} \tanh^{-1}\left(\frac{|w_1|}{\theta \underline{P}_{ci}^{\max}}\right)$  and  $\chi_2(|w_1|) = \left[\frac{|w_1| d_{pgT}}{\theta} \chi_1(|w_1|)\right]^{\frac{1}{2}}$ ,  $\forall w_1 \in (-\theta \underline{P}_{ci}^{\max}, \theta \underline{P}_{ci}^{\max})$ .*

*Proof.* Assuming  $V_6$  as the Lyapunov function, this can be easily proved following same steps as in Theorem III.5.  $\square$

### C. Remarks on Assumptions

1. *Network model*: It was shown in [14] that network dynamics introduces both positive and negative effects on stability in systems with GFCs and SGs. Although algebraic representation of the network gives a conservative stability estimate, the inclusion of network dynamics imposes strict upper bounds on droop feedback gains for ensuring voltage and frequency stability.

2. *AC current limits*: The ac current limits are used to constrain GFC current during faults. We point out that following a fault, typically the reactive component of current increases significantly [15] compared to the real component. As a result, this might not lead to dc-side current saturation. On the other hand, the problem of generation loss leads to increase in real power output and hence dc-side current limit is reached first. Assuming that the available headroom ( $i_{dc}^{max} - i_{dc}$ ) is not very large (which is typical), the ac current limit might not be hit in this condition. If, however this is not the case, then ac-side constraints need to be taken into account in stability analysis, which is outside the scope of the present paper.

3. *Frequency of class-B GFCs*: For class-B GFCs, the working assumption in the 2-bus test system is  $\omega_c \approx \omega_g$ , whereas in the multimachine system, we assume  $\omega_{COI} \approx \omega_{ci}$ ,  $\forall i = 1, 2, \dots, n_1$ . In reality, this may not be true. Also, such models cannot capture the oscillatory electromechanical dynamics present in practical multimachine systems that reflects the angle stability issues.

4. *DC voltage filtering in class-B GFC*: In reality, switching ripple in dc-link voltage can propagate to angle reference through  $\omega_c$  of class-B GFCs. If a low pass filter is used to mitigate this issue, it needs to be considered in the stability analysis.

## IV. RESULTS & DISCUSSIONS

For validating the proposed lemmas and theorems, we consider the test system shown in Fig. 3. To that end, the averaged models shown in Fig. 5 are built in Matlab Simulink and a detailed switched model of a standalone GFC connected to a constant power load  $P_{LC}$  is developed in EMTDC/PSCAD including the control loops shown in Fig.2.

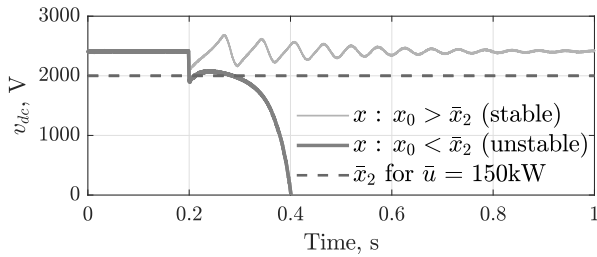


Fig. 7: Class-A GFC: unforced response from PSCAD model.

We validate the ROAs for both classes of GFCs using the PSCAD model by switching the dc bus capacitor voltage to

a value  $x_0$  at  $t = 0.2$  s while operating at equilibrium  $(\bar{x}_1, \bar{u})$ . In Fig. 7, it is shown that for class-A GFC,  $v_{dc}$  collapses if  $x_0 < \bar{x}_2$ , whereas it is stable if  $x_0 > \bar{x}_2$  by slight margin, which validates the ROA defined in Theorem III.1. Figure 8 shows that  $v_{dc}$  returns back to  $\bar{x}_1$  even if it is switched below  $\bar{x}_2$  for class-B GFC.

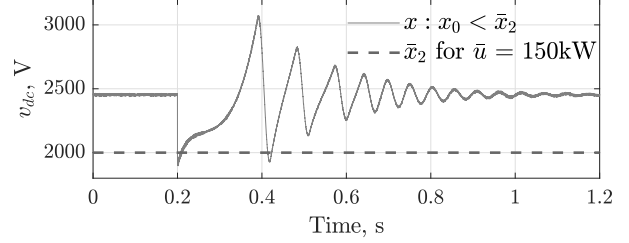


Fig. 8: Class-B GFC: unforced response from PSCAD model.

Next, we validate the ROAs using the average models that capture the dynamics of both SG and GFC. Figure 9 shows the unforced response of these models by initializing  $v_{dc}$  at different values while operating at equilibrium  $(\bar{x}_1, \bar{u})$ . Here, the class-B GFC is stable even when the initial voltage state is significantly lower than  $\bar{x}_2$ .

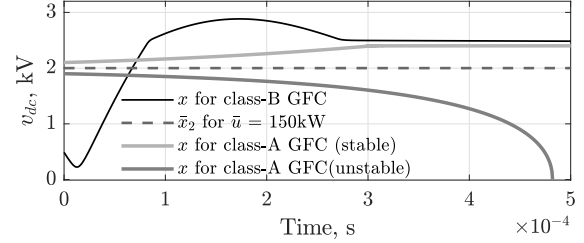


Fig. 9: Unforced response from averaged models.

To validate Theorem III.2, a small step change is given in the load from  $\bar{u} = 175$  kW to  $\bar{u}_m = 177$  kW in PSCAD model of class-A GFC (see, Fig. 10(a)). It can be seen from Fig. 10(b), that the dc voltage is stable. In Fig. 10 (c,d), it is shown that when  $u = \bar{u}_m$ , the unforced response becomes unstable when the initial value of  $x$  is less than  $x_m$ , which proves Theorem III.3.

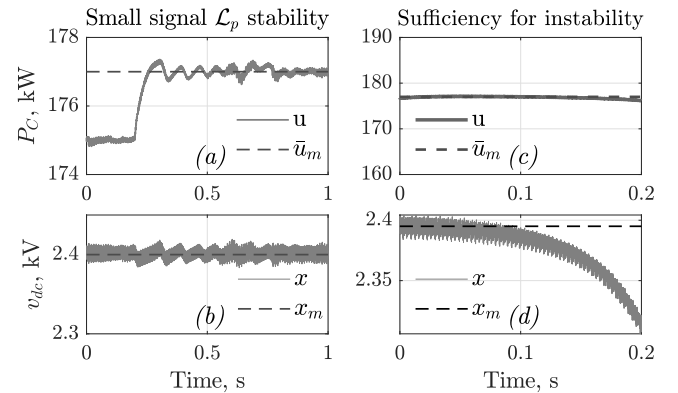


Fig. 10: Class-A GFC PSCAD model: (a),(b): Forced response; (c),(d): Unforced response.

For class-B GFC, a large step change is given in the load from  $\bar{u} = 165$  kW to  $\bar{u}_m = 177$  kW – Fig. 11 confirms the input to state stability per Theorem III.5.

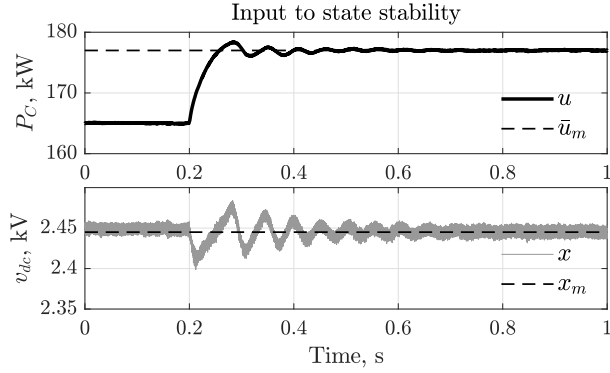


Fig. 11: Power and DC voltage plot for class-B GFC.

## V. CONCLUSION

Stability analysis of power systems consisting of SGs and GFCs with dc-side current limitation showed that the ROA of class-A GFC is a subset of its class-B counterpart. We established the conditions for small-signal finite gain  $\mathcal{L}_p$  stability of class-A GFC and input-to-state state stability of class-B GFC following a bounded variation in the load of the system, and validated the results through simulation studies.

## APPENDIX

$k_c$	1.6e3 $\bar{U}$	$v_{dc}^*$	2.44 kV	$C_c$	8 mF
$G_c$	0.83 $\bar{U}$	$P_c^*$	150 kW	$P_g^*$	150 kW
b	5e3 p.u.	$H_g$	3.7 s	$\tau_g$	5 s
$k_m$	128.75 $V^{-1}$	$\omega^*$	314.16 rad/s	$d_{pg}$	7 p.u.
$d_{pc}$	1e-3 p.u.	$i_{dc}^{max}$	75 A	$P_c^{max}$	178 kW

## REFERENCES

- [1] N. W. Miller, M. Shao, S. Pajic, and R. D'Aquila, "Western wind and solar integration study phase 3-frequency response and transient stability," *National Renewable Energy Lab.(NREL), Golden, CO (United States); GE Energy Management, Schenectady, NY (United States), Tech. Rep.*, 2014.
- [2] EirGrid and Soni, "Ds3: System services review tso recommendations," *EirGrid, Tech. Rep.*, 2012.
- [3] F. Milano, F. Dörfler, G. Hug, D. J. Hill, and G. Verbič, "Foundations and challenges of low-inertia systems (invited paper)," in *2018 Power Systems Computation Conference (PSCC)*, 2018, pp. 1–25.
- [4] M. C. Chandorkar, D. M. Divan, and R. Adapa, "Control of parallel connected inverters in standalone ac supply systems," *IEEE Transactions on Industry Applications*, vol. 29, no. 1, pp. 136–143, 1993.
- [5] Q. Zhong and G. Weiss, "Synchronverters: Inverters that mimic synchronous generators," *IEEE Transactions on Industrial Electronics*, vol. 58, no. 4, pp. 1259–1267, 2011.
- [6] G. Seo, M. Colombino, I. Subotic, B. Johnson, D. Groß, and F. Dörfler, "Dispatchable virtual oscillator control for decentralized inverter-dominated power systems: Analysis and experiments," in *2019 IEEE Applied Power Electronics Conference and Exposition (APEC)*, 2019, pp. 561–566.
- [7] C. Arghir, T. Jouini, and F. Dörfler, "Grid-forming control for power converters based on matching of synchronous machines," *Automatica*, vol. 95, pp. 273–282, 2018, issn: 0005-1098.

- [8] S. Curi, D. Groß, and F. Dörfler, "Control of low-inertia power grids: A model reduction approach," in *2017 IEEE 56th Annual Conference on Decision and Control (CDC)*, 2017, pp. 5708–5713.
- [9] A. Tayyebi, D. Groß, A. Anta, F. Kupzog, and F. Dörfler, "Frequency stability of synchronous machines and grid-forming power converters," *IEEE Journal of Emerging and Selected Topics in Power Electronics*, vol. 8, no. 2, pp. 1004–1018, 2020.
- [10] A. Yazdani and R. Iravani, *Voltage-Sourced Converters in Power Systems: Modeling, Control, and Applications*, ser. Wiley - IEEE. Wiley, 2010.
- [11] Y. Gao, H.-P. Ren, and J. Li, *Grid-forming converters control based on dc voltage feedback*, 2020. arXiv: 2009.05759 [eess.SY].
- [12] A. Tayyebi, A. Anta, and F. Dörfler, *Hybrid angle control and almost global stability of grid-forming power converters*, 2020. arXiv: 2008.07661 [math.OC].
- [13] H. K. Khalil, *Nonlinear systems; 3rd ed.* Prentice-Hall, 2002.
- [14] U. Markovic, O. Stanojev, E. Vrettos, P. Aristidou, and G. Hug, *Understanding stability of low-inertia systems*, Feb. 2019. DOI: 10.31224/osf.io/jwzrq.
- [15] M. G. Taul, X. Wang, P. Davari, and F. Blaabjerg, "Current limiting control with enhanced dynamics of grid-forming converters during fault conditions," *IEEE Journal of Emerging and Selected Topics in Power Electronics*, vol. 8, no. 2, pp. 1062–1073, 2020.